Investigation of dark count rate in NbRe microstrips for single photon detection

Investigation of dark count rate in NbRe microstrips for single photon detection

OPEN ACCESS
IOP Publishing
Superconductor Science and Technology
Supercond. Sci. Technol. **36** (2023) 105011 (9pp)
https://doi.org/10.1088/1361-6668/acf24a

Investigation of dark count rate in NbRe microstrips for single photon detection

P Ercolano[1], C Cirillo[2], M Ejrnaes[3], F Chianese[4], D Salvoni[5], C Bruscino[1], R Satariano[3], A Cassinese[1,6], C Attanasio[7], G P Pepe[1] and L Parlato[1,*]

[1] Dipartimento di Fisica 'E. Pancini', Università degli Studi di Napoli Federico II, I-80125 Napoli, Italy
[2] CNR-SPIN Institute of Superconductors, Innovative Materials and Devices, I-84084 Fisciano, Salerno, Italy
[3] CNR-SPIN Institute of Superconductors, Innovative Materials and Devices, I-80078 Pozzuoli, Italy
[4] Chalmers University of Technology, SE-412 96 Gothenburg, Sweden
[5] Photon Technology (Zhejiang) Co., Ltd Jiashan, Zhejiang, People's Republic of China
[6] Istituto Nazionale di Fisica Nucleare, Sezione di Napoli, P.le Tecchio, 80, 80125 Napoli, Italy
[7] Dipartimento di Fisica 'E. R. Caianiello', Università degli Studi di Salerno, I-84084 Fisciano, Salerno, Italy

E-mail: loredana.parlato@unina.it

Received 11 July 2023, revised 15 August 2023
Accepted for publication 21 August 2023
Published 1 September 2023

Abstract

Superconducting microstrip single photon detectors (SMSPDs) received great interest since they are expected to combine the excellent performance of superconducting nanostrip single photon detectors with the possibility to cover large active areas using low-cost fabrication techniques. In this work, we fabricated SMSPDs based on NbRe to investigate the role of vortices in the dark counts events in this innovative material and in devices with micrometer size. We realized devices with different layouts, namely single microstrips and pairs of parallel microstrips. The energy barriers related to the motion of single vortices or vortex–antivortex pairs, responsible of detection events, have been determined and compared with the ones of similar devices based on different materials, such as MoSi, WSi and NbN. The analysis confirms the high potential of NbRe for the realization of superconducting single photon detectors with large areas.

Keywords: superconducting microstrips single photon detectors, NbRe microstrips, dark counts

(Some figures may appear in colour only in the online journal)

1. Introduction

Thanks to their high performance, superconducting single photon detectors technology is of considerable interest in several fields, such as quantum communication, quantum computing, light detection and ranging (LIDAR), molecular spectroscopy, fluorescence, and so on [1]. In particular, single photon detectors based on nanostrips of superconducting materials (superconducting nanostrip single photon detectors (SNSPDs)) exhibit low dark count rates (DCRs), picosecond time resolution, and near unit efficiency at a wavelength of 1550 nm [1–3]. When an external bias current close to the strip critical current is applied, the appearance of a region with suppressed superconductivity, the so-called hot-spot, with typical diameter $d_{HS} \approx 50 \div 100$ nm [4, 5], forces the current to flow at the edges of this region. It leads locally to a higher supercurrent density, triggering the switch to the resistive state.

* Author to whom any correspondence should be addressed.

For a long time, it was believed that only superconducting strips whose width, w, was comparable with the dimensions of the photon-induced hot-spot can detect single photons. This restricted the study to nanostrips with $w < 150$ nm. However, it was recently predicted that also a wide strip can detect single photons if it is biased at a current close to the depairing current, I_{dep}, with a width $d_{HS} << w < \Lambda$ ($\Lambda = \frac{2\lambda_L^2}{d}$ is the Pearl penetration depth, λ_L and d are the London penetration depth and the thickness of the strip, respectively) [6]. For a relatively thin strip, Λ is of the order of hundreds of μm [7]. Despite this result was experimentally confirmed for superconducting microstrip single photon detectors (SMSPDs) based on NbN, MoSi, and WSi [8–11], the detection mechanisms and the nature of the dark counts in such microstrips are still under investigation. In particular, experiments indicate that vortices play a fundamental role supporting the vortex-assisted detection mechanisms [12]. Indeed, as soon as the strip width exceeds $\approx 4.4\xi_{GL}$, magnetic vortices can exist inside the strip (here ξ_{GL} is the Ginzburg–Landau superconducting coherence length). These can appear both as single vortices (VS), due to an external magnetic field or the magnetic field self-generated by the bias current, and as vortex–antivortex pairs (VAPs), as topological excitations of a two-dimensional (2D) superconducting film [13, 14]. These excitations are particularly frequent in strongly type-II superconductors typically used for SN(M)SPDs. Once a free vortex and/or an antivortex appears in the strip the strong bias current induces a dissipative vortex motion due to the Lorentz force that creates a finite voltage area in the superconductor [15, 16] and successively, due to the thermal instability of these superconductors, to the appearance of a normal state domain [17]. Both mechanisms depend on an energy barrier, which is function of temperature and bias current, and on the properties of the superconductor, such as the coherence length and the London penetration depth.

The research on SMSPDs currently focuses on the exploration of new large area configurations, such as parallel connection of microstrips, as well as on the investigation of innovative superconductors which may work at longer wavelengths. Indeed, this would pave the way to use such detectors in applications where large-area mid-infrared detectors are required, e.g. astronomy, free space quantum communication, LIDAR, etc [18–22]. Recently, NbRe was proposed as a promising material for the fabrication of SN(M)SPDs [23–25]. NbRe-based nanostrips [26] and microstrips [24] have been demonstrated to work as single photon detectors. NbRe is a non-centrosymmetric superconductor, i.e. a system whose crystal structure does not have inversion symmetry. The films available in the literature exhibit a polycrystalline structure with small crystallites ($\sim$3 nm) [27] and disorder-dominated transport properties [28]. In addition, it has a relatively low energy gap which, in principle, may make it capable to detect longer wavelength photons.

In this work, we investigated the origin of dark count rate in single NbRe microstrips and in devices based on two parallel microstrips. In particular, the role of the vortices was investigated in these systems by studying both the behavior of the resistance as function of the temperature, in the framework of the Berezinskii, Kosterlitz and Thouless (BKT) theory [29, 30], and the energy barriers for VS and VAP mechanisms for the DCR [13]. The results obtained of the single strips are compared with the ones of devices based on different materials, such as MoSi, WSi and NbN.

This study aims at a better understanding of two aspects: the role of vortices in micrometric strips with different designs and the effect of the superconducting material chosen as detector.

2. Methods

$Nb_{0.15}Re_{0.85}$ (hereafter NbRe) films of thickness $d = 4$ nm have been deposited on Si/SiO_x substrate by DC magnetron sputtering in ultra-high vacuum (pressure $\sim 10^{-8}$ mbar) at room temperature. The deposition was performed in an Ar pressure of $4 \cdot 10^{-3}$ mbar at a growth rate of 0.3 nm s^{-1}. The NbRe surface was then protected by a 2 nm thick Al cap layer. The samples were patterned through optical lithography by direct writing through smart printing. Then, the pattern was transferred to the superconducting layer by argon ion etching, with a dig rate of 1 nm min^{-1} [24].

We have fabricated two different chips (samples A and B) with microstrips whose nominal widths, w, range from 1 to 2.5 μm, and whose lengths, L, range from 5 to 12.5 μm. The devices have different geometries: single microstrips (figure 1(a)) and pairs of parallel microstrips (figure 1(b)) to increase the detection area without increasing the kinetic inductance. In both configurations, patterns with rounded corners were realized in order to reduce the current crowding effect. In addition, in order to correctly evaluate the low temperature resistivity, ρ_n, bridges with four probe geometry were realized.

Electric transport measurements were performed in a ^{4}He cryostat with a four-probe technique by using the same procedure described elsewhere [24]. The critical temperature, T_c, was experimentally estimated by resistance-temperature $[R(T)]$ curves as the temperature in the middle of the transition between the normal and the superconducting state and, therefore, indicated as T_c^{half}. The critical current, I_c, was defined as the maximum current of the current–voltage (IV) curve before the switching to the resistive branch. For DCR measurements we used a different experimental setup equipped with another dip probe in a Dewar endowed with an Al shield and three mu-metal shields to reduce the background DCR. In this setup the temperature is controlled by pumping on the liquid helium bath where the probe is immersed. The SMSPDs are electrically connected through a small printed circuit to a coaxial cable that goes to room temperature where a bias-tee (Mini-circuits ZFBT-6GW+) allows us to both apply a noise filtered DC current bias from a custom low noise electronics and amplify the SMSPD signal pulses using an RF amplifier (Mini-circuits ZFL-1000LN) with gain of 20 dB, bandwidth between 0.1 MHz and 1000 MHz. The counting rate is measured by an electronic counter (Hewlett-Packard 5316B). The voltage pulses can be monitored and acquired by an oscilloscope (Keysight DSO6014A), having a bandwidth of 1 GHz

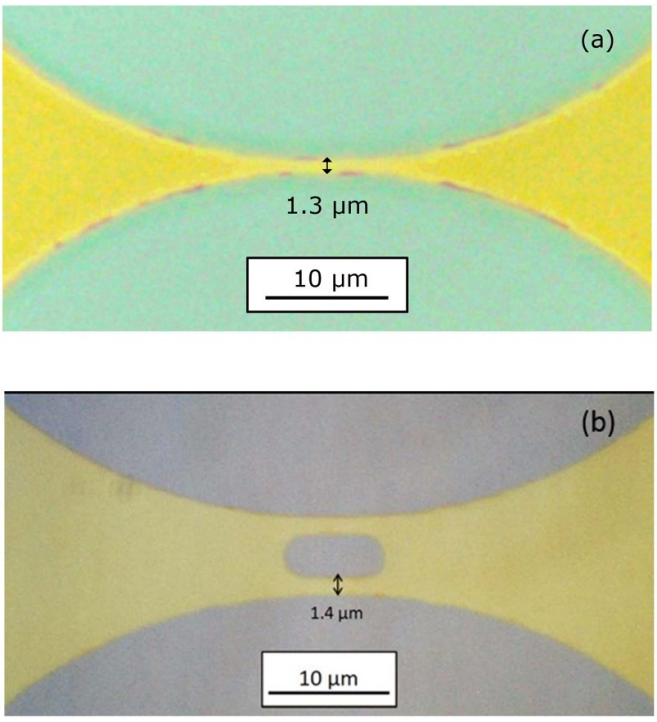

Figure 1. Microscope photo of an NbRe single strip (a) and of a pair of parallel strips (b) realized by optical lithography.

and a sampling rate of 4 GSa s^{-1} connected to the computer. Since the microstrips feature small kinetic inductance, they are more affected by the latching effect, i.e. the superconducting regime does not spontaneously restore after the switching event [31, 32]. Hence, an additional inductor (470 nH) and a parallel resistor (333 Ω for sample A and 15.9 Ω for sample B) are used to overcome this problem.

3. Theoretical models

As demonstrated in [24], NbRe microstrips can work as single photon detectors at $T = 2$ K. At this temperature it is reasonable to assume that thermally activated processes are dominating with respect to quantum-mechanical tunneling events, and hence to consider only the former as origin of DCR [12, 33, 34]. They occur by overcoming an energy barrier $U(T, I_b)$, so that DCR can be expressed through the Boltzmann factor [13]:

$$DCR(T, I_b) \sim \exp\left(-\frac{U(T, I_b)}{k_B T}\right), \tag{1}$$

where k_B is the Boltzmann constant.

Since in NbRe films the zero-temperature superconducting coherence length ξ is about 5 nm [28], both the conditions $d \leq \xi$ and $w >> \xi$ are verified at $T = 2$ K. For these reasons, the system can be considered 2D rather than one-dimensional, and therefore processes involving vortices have been taken into account [14]. According to the BKT theory, a transition temperature, T_{BKT}, is defined such that, when $T < T_{BKT}$, all vortices and antivortices are bound and not free to move. Therefore, the resistance of the strip is strictly zero, as there is no dissipation [13]. When the temperature exceeds T_{BKT}, VAPs begin to dissociate, so both couples of vortices and VS are present. Decoupled vortices move due to the Lorentz force generated by the bias current, and the effect of this process is the appearance of a non-zero resistance for $T_{BKT} < T < T_c$ equal to:

$$R(T) = a \exp\left(-2\sqrt{b\frac{T_c - T}{T - T_{BKT}}}\right). \tag{2}$$

Here b quantifies the efficacy of this effect and depends on the material, and a is the resistance at $T = T_c$ and depends also on the geometry of the system [13].

The expression of the energy barrier for the breaking of a VAP is [13]:

$$U_{VAP}(T, I_b) = \frac{A(T, I_b)}{\varepsilon}\left[\ln\left(\frac{2.6 I_c(T)}{I_b}\right) - 1 + \frac{I_b}{2.6 I_c(T)}\right], \tag{3}$$

where ε is the mean polarizability of VAPs and $A(T, I_b)$ is the interaction constant between the vortices, which can be expressed as $A(T, I_b) = \frac{\Phi_0^2}{\pi \mu_0 \tilde{\Lambda}(T, I_b)}$ [13]. Here Φ_0 is the magnetic flux quantum and μ_0 is the vacuum permeability. $\tilde{\Lambda}$ is the renormalized Pearl length, which depends both on the temperature and the bias current [16, 35]: $\tilde{\Lambda}(T, I_b) = \beta(I_b)\Lambda(T)$, where $\beta(I_b)$ is equal to 1 when I_b is zero and to 1.157 when $I_b = I_c$. In this model, the expression of DCR due to VAPs breaking is:

$$DCR_{VAP}(T, I_b) = \alpha_{VAP} \exp\left(-\frac{U_{VAP}(T, I_b)}{k_B T}\right), \tag{4}$$

where α_{VAP} is the attempt rate [13].

Conversely, VS are formed at the edge of the strip by the effect of the magnetic self-field, and they can move perpendicularly to I_b, giving rise to a normal domain which may result in a dark count. This process occurs when the energy barrier for the vortex entry, i.e. U_{VS}, is overcome, where [13]:

$$U_{VS}(T, I_b) = -E_B(T, I_b)\left\{\ln\left[\frac{\pi\xi(T)}{2w}\sqrt{1 + \left[\frac{I_b}{I_B(T, I_b)}\right]^2}\right] + \frac{I_b}{I_B(T, I_b)}\left[\arctan\left(\frac{I_B(T, I_b)}{I_b}\right) - \frac{\pi\xi(T)}{2w}\right]\right\}. \tag{5}$$

Here $I_B(T, I_b) = \frac{\Phi_0}{2\mu_0 \tilde{\Lambda}(T, I_b)}$ is the scale current and E_B is the scale energy, which can be written as $E_B(T, I_b) = \frac{I_B \Phi_0}{\pi}$ [13]. According to this model, the expression of DCR due to VS is [13]:

$$DCR_{VS}(T, I_b) = \alpha_{VS} I_b \exp\left(-\frac{U_{VS}(T, I_b)}{k_B T}\right), \tag{6}$$

where α_{VS} is a proportionality constant. In this case the attempt rate, $\alpha_{VS} I_b$, is proportional to the bias current because the magnetic self-field is proportional to I_b.

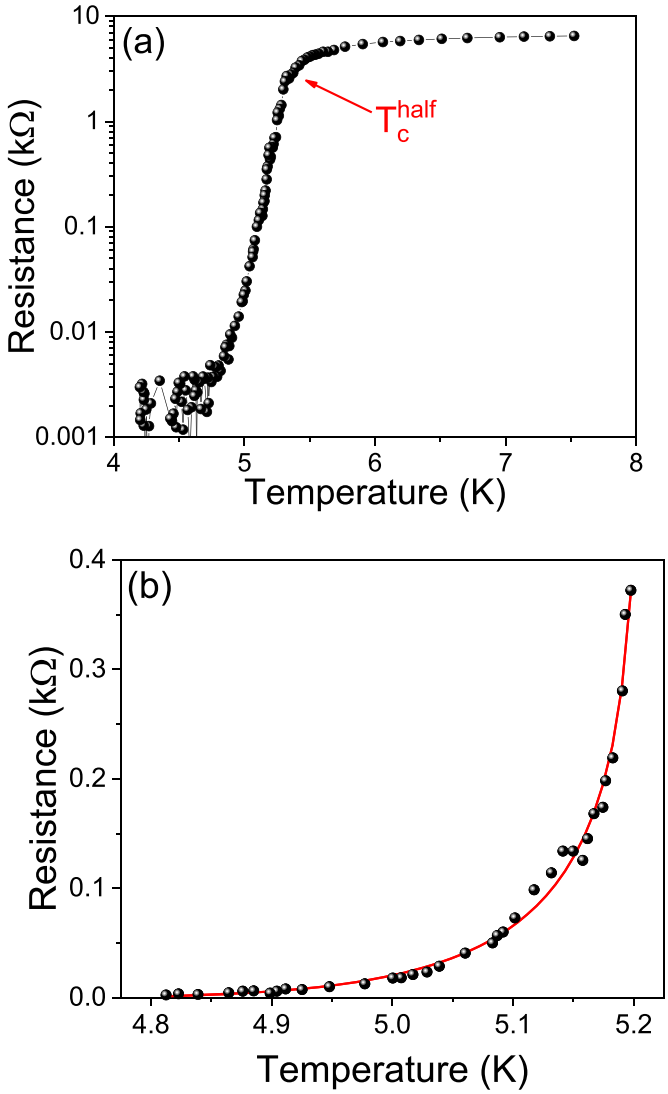

Figure 2. (a) $R(T)$ curve for device B1. The red arrow indicates the critical temperature T_c^{half}. (b) R (T) curve in the low voltage region (points) along with the fitting curve according to BKT theory (line) in the region $T_{BKT} < T < T_c$.

4. Experimental results and discussion

Our analysis started from measurements of the two test strips (A1 from sample A and B1 from sample B) patterned in a four-terminal bridge. First, we evaluated the low temperature resistivity as $\rho_n^{A1} = (150 \pm 10)\,\mu\Omega$ cm and $\rho_n^{B1} = (110 \pm 10)\,\mu\Omega$ cm for devices A1 and B1, respectively.

In order to investigate the role of the vortices in our devices, we analyzed the $R(T)$ curve of the bridges. The $R(T)$ transition of the bridge B1 in shown in figure 2(a) in semilog scale, where the critical temperature, $T_c^{half,B1} = (5.4 \pm 0.1)\,K$, is indicated by a red arrow. The same procedure was performed for the bridge A1 for which $T_c^{half,A1} = (5.2 \pm 0.1)\,K$. A fitting procedure according to equation (2) was performed for both strips by leaving T_c, T_{BKT}, together with a and b as fitting parameters. The resulting fitting curve for device B1 is shown by the red curve in figure 2(b). The good agreement between the theory and the experimental points indicates that vortices play a key role in the microstrips.

From the previous analysis, by using the measured values of ρ_n and the ones of T_c resulting from the fitting procedure, it is therefore possible to derive the London penetration depth at zero temperature as $\lambda_L(0) = 1.05 \cdot 10^{-3}\sqrt{\frac{\rho_n}{T_c}}$ [30]. It results that $\lambda_L^{A1}(0) = (570 \pm 20)\,nm$ and $\lambda_L^{B1}(0) = (480 \pm 30)\,nm$. The superconducting coherence length at zero temperature $\xi(0)$ is usually estimated from critical magnetic field measurements. In [28] for an NbRe film 60 nm thick it is $T_c{}^{half} = (7.3 \pm 0.1)\,Knm$ and $\xi(0) = (4.8 \pm 0.1)$. In order to estimate $\xi(0)$ for our samples, we use the relation $\xi^{I}(0)\sqrt{T_c^{I}} = \xi^{II}(0)\sqrt{T_c^{II}}$ [36], which correlates the value of T_c and $\xi(0)$ for different samples (identified by the superscriptions I and II) of the same material. In our case we obtain $\xi^{A1}(0) = (5.7 \pm 0.2)\,nm$ and $\xi^{B1}(0) = (5.7 \pm 0.2)\,nm$ for devices A1

Table 1. Summary of the characteristics of the bridges A1 and B1, along with the fitting results obtained in the framework of the BKT model.

Device	Geometry	d (nm)	w (μm)	L (μm)	ρ_n ($\mu\Omega$ cm)	a (kΩ)	b	T_c (K)	T_{BKT} (K)	$\lambda_L(0)$ (nm)	$\xi(0)$ (nm)
A1	Single strip	4	2.5	12.5	150 ± 10	1.9 ± 0.4	9 ± 6	5.14 ± 0.06	4.92 ± 0.08	570 ± 20	5.7 ± 0.2
B1	Single strip	4	6.7	7.5	110 ± 10	0.54 ± 0.09	6 ± 4	5.2 ± 0.1	4.8 ± 0.3	480 ± 30	5.7 ± 0.2

Table 2. Devices under consideration and their characteristics. The values of J_c are measured at two contacts in the measurement configuration described in section II, and at the operation temperature, which is 1.79 K ($T/T_c = 0.35$) and 1.57 K ($T/T_c = 0.30$) for devices A2 and B2, respectively.

Device	Geometry	d (nm)	w (μm)	L (μm)	$A = wL$ (μm^2)	$J_c(T)$ (MA cm^{-2})
A2	Single strip	4	1.3	5	6.5	1.55
B2	Pair of parallel strips	4	1.4	5	14.0	2.79

and B1, respectively. The values of these quantities at the operation temperature can be obtained by assuming a temperature dependence according to $\lambda_L(T) = \frac{\lambda_L(0)}{\sqrt{1-\left(\frac{T}{T_c}\right)^4}}$ and $\xi(T) = \frac{\xi(0)}{\sqrt{1-\frac{T}{T_c}}}$. The resulting fitting parameters, as well as the main characteristics of both bridges, are reported in table 1.

The analysis of DCR was performed on a single strip (A2, figure 1(a)) and a pair of parallel strips (B2, figure 1(b)) with similar widths, namely $w = 1.3$ μm and $w = 1.4$ μm, respectively. In table 2 their main characteristics are reported. We evaluated their sensitive area for detection, $A = wL$. Measured IV curves at two different temperatures are shown in the insets of figure 3. We note that the curves appear very different because the parallel resistor used for device B was low enough that when the bias current exceeds the critical current relaxation oscillations appear, with a low average voltage value, that strongly reduce the hysteresis. This does not occur for device A which instead switches directly to the fully resistive state and thus exhibit strong hysteresis. The critical current density, J_c, has been determined as $J_c = I_c/S$, where $S = wd$ is the cross-section of the microstrip. The values obtained at the lowest measuring temperatures, namely 1.79 K ($T/T_c = 0.35$) for device A2 and 1.57 K ($T/T_c = 0.30$) for device B2, are reported in table 2.

We now focus on the behavior of DCR versus I_b/I_c for the single strip A2 and we observe a behavior that can be attributed to a single thermally activated process [37], which is shown in figure 4 in a semilog scale. In order to study these data in the framework of equation (1) and infer some information about these devices, the theoretical models described previously have been taken into account. Since we consider only currents near to the critical one, we assume that the factor β in $\tilde{\Lambda}(T, I_b)$ is constant and equal to its value at I_c, namely 1.157. Therefore, a fitting procedure, according to equations (4) and (6), has been performed using as free parameters α_{VAP}, ε, and α_{VS}. Their values are reported in table 3. Both models well fit the experimental data (see figure 4), so both mechanisms (and any linear combination) can be present. It is worth to note that, for the VS model, no fitting parameter was used for the evaluation of the energy barrier U_{VS}, and the only fitting parameter is the proportionality constant α_{VS}. Concerning the VAP model, the fit gives an estimate of ε, which is a quantity difficult to access experimentally. The obtained value, $\varepsilon = 1.48 \pm 0.01$, is in line with what is reported for other materials [7, 33].

According to equations (3) and (5), it is possible to evaluate the energy barriers which characterize the two processes under consideration. A comparison with single microstrips of other materials in a similar temperature condition ($T \approx 0.4T_c$) is shown in figure 5. We consider a MoSi device (fabricated as in [38]) and other two, based on NbN and WSi, from the literature [8, 11], respectively. We performed on the MoSi microstrip the same DCR measurement as on the NbRe one, and then we retrieved the coherence length and the London penetration depth from literature [9]. For the NbN and WSi devices, we took the DCR values reported in [8, 11], respectively. Then, we used the values of $\lambda_L(0)$ and $\xi(0)$ reported in [4, 8] for NbN and in [39] for WSi. In this way, the same analysis as A2 was performed, obtaining the energy barriers. In order to compare the devices, the energies have been plotted as a function of the bias current normalized to the critical current at their working temperature (figure 5). It can be observed in table 4 that the energy barriers verify the same property for which $U_{VS} > U_{VAP}$.

The barriers estimated by the DCRs underlying the vortex-based models can give indications on the sensitivity to detect photons in different materials, too. In order to make a more quantitative comparison among the SMSPDs of different materials, we have referred to the hot-spot two-temperature model developed by Vodolazov [6]. According to this model, the absorption of a photon results in the hot-spot region in which the electronic system has an initial effective temperature T_{init} higher than working temperature T of the remaining strip. At a fixed T_{init} there is a current I_{det} such that, if the current in the strip is higher than this threshold, the photon is detected. The detection mechanism involves vortex entry or VAPs depending on the position of the hot-spot in the strip. When the hot-spot appears near the edge of the strip, a vortex enters the region where superconductivity is suppressed and passes across the strip. Conversely, when the hot-spot appears in the middle of the strip, a vortex and an antivortex form in it and cross the strip moving in opposite directions. As described above, these effects lead to the formation of a normal domain

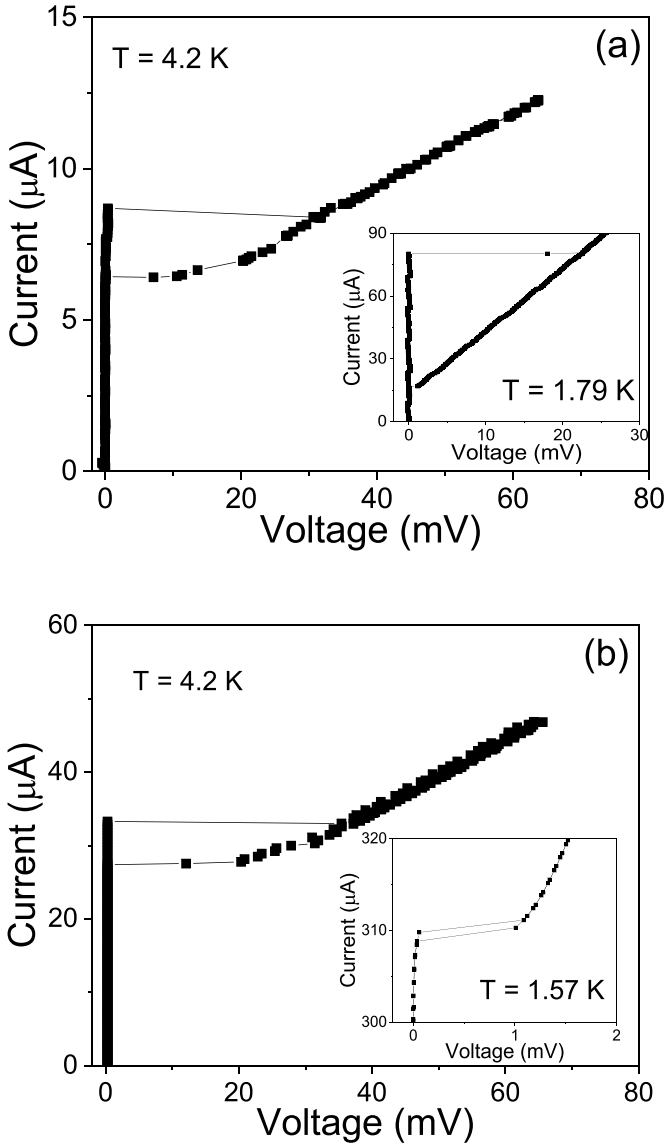

Figure 3. Current–voltage characteristics at $T = 4.2$ K of device A2 (a) and B2 (b), respectively. In measuring both, the inductor of 470 nH was present in series. The inset of panel a (b) shows the IV curves at $T = 1.79$ K ($T = 1.57$ K). In the case of A2, the parallel resistor of 333 Ω was added, whereas in the case of B2, the resistor of 15.9 Ω was added.

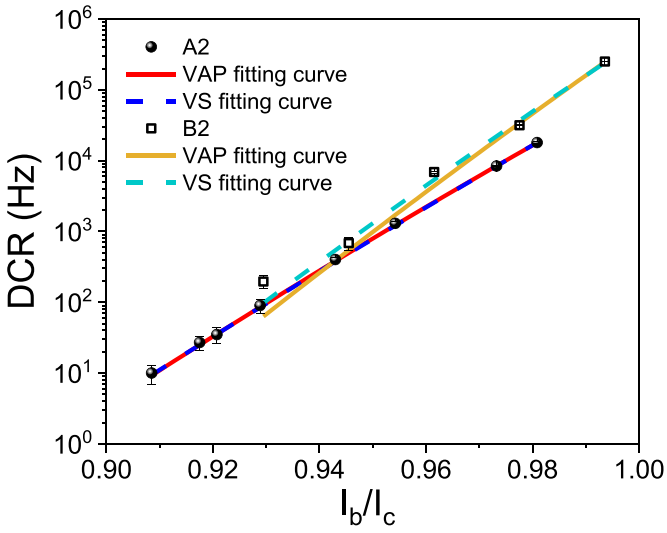

Figure 4. DCR vs the normalized bias current for the single strip A2 (black solid circles) and the pair of parallel strips B2 (black open squares), at $T = 1.79\,K$ and $T = 1.57\,K$ respectively. The solid and dashed lines are the VAP (equation (4)) and VS (equation (6)) fitting curves, respectively.

and thus to the registration of a count. If the current does not exceed $I_{\rm det}$, even if these processes can take place, the heating due to movement of vortices is not enough to compensate for the cooling due to the diffusion of the electrons and therefore no event is recorded. This current threshold depends on the initial effective temperature of the hot-spot, which is determined by the energy of the incident photon $E_{\rm photon}$ and by the characteristics of the superconductor expressed by the parameter γ [6]:

$$\gamma = \frac{8\pi^2}{5}\frac{C_{\rm e}}{C_{\rm ph}}\bigg|_{T_{\rm c}}, \tag{7}$$

where $C_{\rm e}$ ($C_{\rm ph}$) is the electronic (phononic) specific heat capacity. The parameter γ quantifies the energy fraction of the absorbed photon which is retained by the electronic system, and it is also related to the thermalization time $\tau_{\rm th}$ of the electrons. As γ increases, the ability to detect photons improves. Indeed, if $\tau_{\rm th}$ is larger than the diffusion time $\tau_{\rm D}$, the energy of the absorbed photon is spread over a large area before it is removed from the electronic system. Therefore, absorption changes the superconducting properties, and thus on the effective temperature of the electronic system, across a larger area. Analogously, the higher the photon energy absorbed by the electronic system, the greater its effect on the superconducting properties [6]. In this sense the material characteristics play a crucial role also since the photon energy must be compared to the characteristic energy $E_0{\xi_{\rm c}}^2 d$ of the electronic system, where $E_0 = 4N(0)\,(k_{\rm B}T_{\rm c})^2$ and $\xi_{\rm c} = \sqrt{\hbar D/k_{\rm B}T_{\rm c}}$ [6, 40]. Here $N(0)$ is the one-spin density of states of electrons in the normal state at the Fermi energy, $\hbar$ is the reduced Planck constant, and D is the diffusion coefficient. E_0 represents the difference between the energy density in the normal and superconducting state, and ${\xi_{\rm c}}^2 d$ is the characteristic volume of the initial hot-spot [6]. Therefore, in order to compare devices made of different materials, we have taken into account the energy $E_0{\xi_{\rm c}}^2 d$ and the parameter γ. The samples under consideration and the results relating to them are reported in table 4. Although these devices have different geometrical parameters, it is relevant to note that the energy $E_0{\xi_{\rm c}}^2 d$ of NbRe is lower than for amorphous materials and similar to NbN, even if lower values of energy barriers are estimated. Moreover, γ is comparable with the high values reported for amorphous materials. For these reasons we expect that NbRe devices, compared to NbN ones can be suitable to detect longer wavelength photons. Indeed, a higher γ implies that less energy of the photon is dispersed in the phononic system and therefore is better retained by the electronic one, having a greater effect on the suppression of superconductivity.

Table 3. Results of the fit on DCR for devices A2 and B2.

		VAP model fitting parameters		VS model fitting parameters
Device	Geometry	$\ln(\alpha_{VAP})$ [$\ln(Hz^{-1})$]	ε	$\ln(\alpha_{VS})$ [$\ln(Hz^{-1}\ A^{-1})$]
A2	Single strip	(64.4 ± 0.3)	1.48 ± 0.01	(136.152 ± 0.002)
B2	Pair of parallel strips	(80 ± 3)	1.89 ± 0.08	(82.80 ± 0.04)

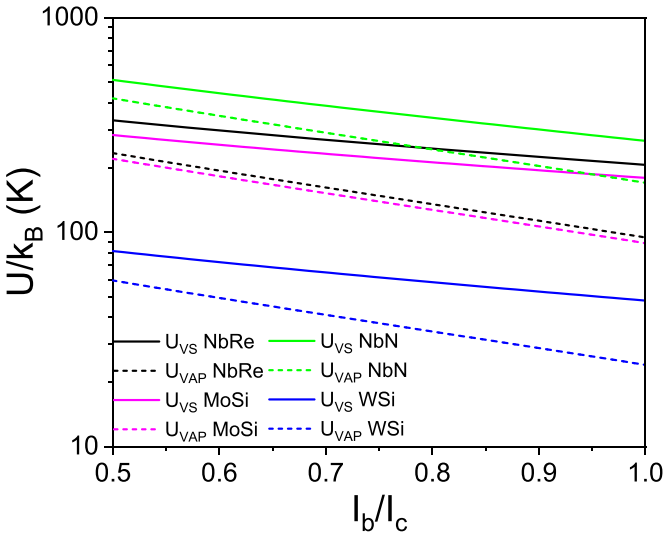

Figure 5. Energy barriers for an NbRe microstrip with $w = 1.3$ μm (black lines), a MoSi microstrip with $w = 1.6$ μm (magenta lines) [38], an NbN microstrip with $w = 2.12$ μm (green lines) [8] and a WSi microstrip with $w = 1$ μm (blue lines) [11] at $T \approx 0.4$ T_c.

Table 4. Comparison of the device characteristics and the microscopical parameters extracted from the DCR analysis for the different superconducting materials considered in this study.

Material	w (μm)	d (nm)	$\frac{T}{T_c}$	U_{VAP}/k_B (K) @$I_b = 0.99I_c$	U_{VS}/k_B (K) @$I_b = 0.99I_c$	$E_0\xi_c{}^2 d$ (meV)	γ
NbRe[a]	1.3	4	0.35	96	207	10.07	93
MoSi[b]	1.6	5	0.43	90	180	5.27	83
WSi[c]	1	2.1	0.28	24	48	2.08	89
NbN[d]	2.12	5.8	0.49	173	269	8.85	10

[a] Data from [23, 24].
[b] Data from [9, 33, 43].
[c] Data from [11, 39, 40, 44].
[d] Data from [4, 8, 45].

Finally, we investigated the dark count rate in the pair of parallel microstrips. The comparison of DCR in devices A2 and B2 is shown in figure 4 in a semilog scale. The DCR of the pair of parallel strips B2 is about twice the one of the single strip A2. Keeping in mind that both devices under consideration have the same length and comparable width, this result can be interpreted considering that the switching of one of the two strips of samples B2 causes the switching of the other one [41, 42], namely the transition of one strip is enough to record a dark count. This observation is compatible with both the VAP and VS models as, according to the former, DCR is proportional to the length of the strip, while according to the latter it is proportional to its sensitive area [12] and in both cases we expect an increase in the DCR of a factor two. This is also true if there is a distribution of constrictions that is similar for both devices.

The analysis performed on the single microstrip was carried out for the pair of parallel microstrips, too. As for the single strips, both VAP and VS models are able to fit the trend of the experimental data. The results of the fitting procedure are reported in table 3. The fitted parameter ε is of the same order of the single NbRe microstrip, but in the case of a pair of microstrips we observe a light increase. According to equations (3) and (5), it is possible to study the trend of the energy barriers of VAP and VS processes for B2 and compare it with the one of A2. In figure 6, it is observed that the barriers behave differently in the two devices with different geometry. Indeed, in the pair of parallel strips U_{VAP} and U_{VS} have

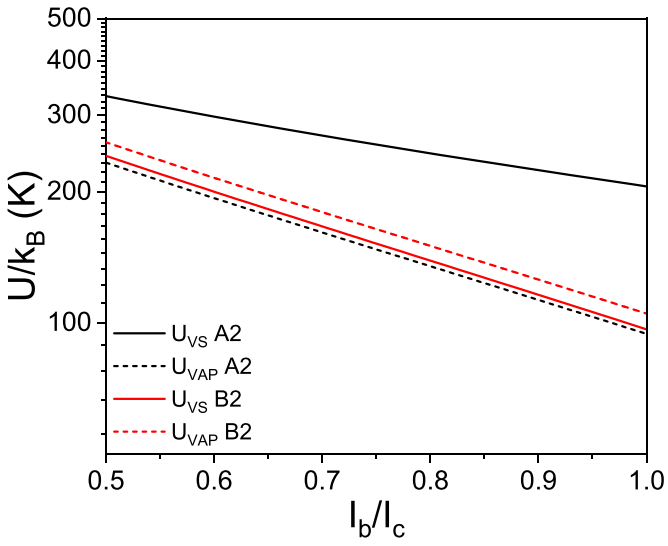

Figure 6. Energy barriers for the single strip A2 (black lines) and the pair of parallel strips B2 (red lines), at $T = 1.79\,K$ and $T = 1.57\,K$, respectively. Continuous (dashed) lines correspond to VS (VAP) processes.

a similar height as their relative difference is about 8% when $I_b = 0.99 I_c$, while for the single strip U_{VS} is about twice U_{VAP} at the same $\frac{I_b}{I_c}$ ratio. Although a lower energy barrier implies a higher DCR, it also results in an enhanced detection efficiency. Further analysis of measurements of the photoresponse or DCR in the presence of a magnetic field might explain these aspects.

5. Conclusions

We reported on the study of the dark counts and the energetic barriers of NbRe microstrips used as single photon detectors. The micrometric dimensions allow the covering of large areas without the limitations of a long recovery time, and the fruition of the advantages of the use of optical lithography techniques. Here, we fabricated devices with different geometries, namely single strips and pairs of parallel strips. The analysis of the $R(T)$ curves and DCR has highlighted the importance of the role played by vortices in these devices, in accordance with the theoretical predictions. According to the VAP and VS models, from the characteristics of the devices, the behavior of DCR was estimated and it fits the trend of the experimental points. The energy barriers of the single microstrip have been compared with the results from literature on similar devices realized with different materials. It emerged that the activation energies for the processes involving VAP and VS have the same behavior, namely $U_{VS} > U_{VAP}$. In addition, the analysis according to the hot-spot two-temperature model has showed that NbRe can be included among the materials used for the realization of single photon detectors since the energy of an absorbed photon is effectively retained by the electronic system. Finally, we compared the results obtained on the single microstrip with the ones of the pair of parallel microstrips. It turned out that the difference in this case is that $U_{VS} \approx U_{VAP}$. In addition, the pair of parallel strips has a detection area double than the single strip and a lower recovery time thanks to a reduction of the kinetic inductance.

Data availability statement

All data that support the findings of this study are included within the article (and any supplementary files).

Acknowledgments

This research was supported by the QUANCOM Project 225521 (MUR PON Ricerca e Innovazione No. 2014–2020 ARS01_00734).

Conflict of interest

The authors have no conflicts to disclose.

ORCID iDs

C Cirillo https://orcid.org/0000-0001-8755-4484
L Parlato https://orcid.org/0000-0002-1646-3435

References

[1] You L 2020 *Nanophotonics* **9** 2673
[2] Zadeh I E, Chang J, Los J W N, Gyger S, Elshaari A W, Steinhauer S, Dorenbos S N and Zwiller V 2021 *Appl. Phys. Lett.* **118** 190502
[3] Pepe G P *et al* 2009 *Cryogenics* **49** 660
[4] Zhang X, Engel A, Wang Q, Schilling A, Semenov A, Sidorova M, Hübers H W, Charaev I, Ilin K and Siegel M 2016 *Phys. Rev.* B **94** 174509
[5] Heeres R W and Zwiller V 2012 *Appl. Phys. Lett.* **101** 112603
[6] Vodolazov D Y 2017 *Phys. Rev. Appl.* **7** 034014
[7] Nasti U, Parlato L, Ejrnaes M, Cristiano R, Taino T, Myoren H, Sobolewski R and Pepe G P 2015 *Phys. Rev.* B **92** 014501
[8] Korneeva Y P, Vodolazov D Y, Semenov A V, Florya I N, Simonov N, Baeva E, Korneev A A, Goltsman G N and Klapwijk T M 2018 *Phys. Rev. Appl.* **9** 064037
[9] Korneeva Y P, Manova N N, Florya I N, Mikhailov M Y, Dobrovolskiy O V, Korneev A A and Vodolazov D Y 2020 *Phys. Rev. Appl.* **13** 024011
[10] Charaev I, Morimoto Y, Dane A, Agarwal A, Colangelo M and Berggren K K 2020 *Appl. Phys. Lett.* **116** 242603
[11] Chiles J, Buckley S M, Lita A E, Verma V B, Allmaras J, Korzh B, Shaw M D, Shainline J M, Mirin R P and Nam S W 2020 *Appl. Phys. Lett.* **116** 242602
[12] Engel A, Renema J J, Il'in K and Semenov A 2015 *Supercond. Sci. Technol.* **28** 114003
[13] Bartolf H, Engel A, Schilling A, Il'in K, Siegel M, Hübers H W and Semenov A 2010 *Phys. Rev.* B **81** 024502
[14] Bell M, Sergeev A, Mitin V, Bird J, Verevkin A and Goltsman G 2007 *Phys. Rev.* B **76** 094521
[15] Zotova A N and Vodolazov D Y 2012 *Phys. Rev.* B **85** 024509
[16] Bulaevskii L N, Graf M J, Batista C D and Kogan V G 2011 *Phys. Rev.* B **83** 144526
[17] Ejrnaes M, Casaburi A, Mattioli F, Leoni R, Pagano S and Cristiano R 2010 *Phys. Rev.* B **81** 132503
[18] Polakovic T, Armstrong W, Karapetrov G, Meziani Z E and Novosad V 2020 *Nanomaterials* **10** 1198

[19] Taylor G G, Morozov D, Gemmell N R, Erotokritou K, Miki S, Terai H and Hadfield R H 2019 *Opt. Express* **27** 38147
[20] Verma V B *et al* 2021 *APL Photonics* **6** 056101
[21] Salvoni D, Boselli A, Sannino A, Parlato L, Ejrnaes M, Zhang C, You L, Wang X, Amoruso S and Pepe G P 2021 *Chem. Eng. Trans.* **84** 175
[22] Salvoni D *et al* 2022 *IEEE Trans. Appl. Supercond.* **32** 1–4
[23] Caputo M, Cirillo C and Attanasio C 2017 *Appl. Phys. Lett.* **111** 192601
[24] Ejrnaes M, Cirillo C, Salvoni D, Chianese F, Bruscino C, Ercolano P, Cassinese A, Attanasio C, Pepe G P and Parlato L 2022 *Appl. Phys. Lett.* **121** 262601
[25] Cirillo C, Caputo M, Parlato L, Ejrnaes M, Salvoni D, Cristiano R, Pepe G P and Attanasio C 2020 *Low Temp. Phys.* **46** 379
[26] Cirillo C, Chang J, Caputo M, Los J W N, Dorenbos S, Zadeh I E and Attanasio C 2020 *Appl. Phys. Lett.* **117** 172602
[27] Cirillo C, Caputo M, Divitini G, Robinson J W A and Attanasio C 2022 *Thin Solid Films* **758** 139450
[28] Cirillo C, Carapella G, Salvato M, Arpaia R, Caputo M and Attanasio C 2016 *Phys. Rev.* B **94** 104512
[29] Berezinskii L 1970 *Zh. Eksp. Teor. Fiz.* **59** 907
[30] Kosterlitz J M and Thouless D J 1973 *J. Phys.* C **6** 1181
[31] Kerman A J, Yang J K W, Molnar R J, Dauler E A and Berggren K K 2009 *Phys. Rev.* B **79** 100509
[32] Ejrnaes M, Casaburi A, Cristiano R, Quaranta O, Marchetti S and Pagano S 2009 *J. Mod. Opt.* **56** 390–4
[33] Salvoni D *et al* 2020 *Phys. Rev. Appl.* **18** 014006
[34] Parlato L *et al* 2020 *J. Low Temp. Phys.* **199** 6
[35] Bulaevskii L N, Graf M J and Kogan V G 2012 *Phys. Rev.* B **85** 014505
[36] Draskovic J, Lemberger T R, Peters B, Yang F, Ku J, Bezryadin A and Wang S 2013 *Phys. Rev.* B **88** 134516
[37] Ejrnaes M *et al* 2019 *Sci. Rep.* **9** 8053
[38] Salvoni D *et al* 2022 *IEEE 15th Workshop on Low Temperature Electronics (WOLTE)* (https://doi.org/10.1109/WOLTE55422.2022.9882683)
[39] Zhang X, Lita A E, Liu H, Verma V B, Zhou Q, Nam S W and Schilling A 2021 *Commun. Phys.* **4** 100
[40] Colangelo M *et al* 2022 *Nano Lett.* **22** 5667
[41] Ejrnaes M, Casaburi A, Quaranta O, Marchetti S, Gaggero A, Mattioli F, Leoni R, Pagano S and Cristiano R 2009 *Supercond. Sci. Technol.* **22** 055006
[42] Ejrnaes M, Cristiano R, Quaranta O, Pagano S, Gaggero A, Mattioli F, Leoni R, Voronov B and Goltsman G 2007 *Appl. Phys. Lett.* **91** 262509
[43] Lita A E, Verma V B, Chiles J, Mirin R P and Nam S W 2021 *Supercond. Sci. Technol.* **34** 054001
[44] Sidorova M V, Kozorezov A G, Semenov A V, Korneeva Y P, Mikhailov M Y, Devizenko A Y, Korneev A A, Chulkova G M and Goltsman G N 2018 *Phys. Rev.* B **97** 184512
[45] Engel A, Aeschbacher A, Inderbitzin K, Schilling A, Il'in K, Hofherr M, Siegel M, Semenov A and Hübers H W 2012 *Appl. Phys. Lett.* **100** 062601